Front. Med. 2025, 19(2): 318−328
https://doi.org/10.1007/s11684-024-1122-2

RESEARCH ARTICLE

CHAF1B promotes the progression of lung squamous-cell carcinoma by inhibiting *SETD7* expression

Zhuo Zheng[1,2], Yongfang Lin[2], Hua Guo[2], Zheng Liu[2], Xiaoliang Jie[2], Guizhen Wang[2], Guangbiao Zhou (✉)[1,2]

[1]Guizhou University Medical College, Guiyang 550025, China; [2]State Key Laboratory of Molecular Oncology, National Cancer Center/National Clinical Research Center for Cancer/Cancer Hospital, Chinese Academy of Medical Sciences and Peking Union Medical College, Beijing 100021, China

Abstract **The p60 subunit of the chromatin assembly factor-1 complex, that is, chromatin assembly factor-1 subunit B (CHAF1B), is a histone H3/H4 chaperone crucial for the transcriptional regulation of cell differentiation and self-renewal. *CHAF1B* is overexpressed in several cancers and may represent a potential target for cancer therapy. However, its expression and clinical significance in lung squamous-cell carcinoma (LUSC) remain unclear. In this study, we performed weighted gene correlation network analysis to analyze the Gene Expression Omnibus GSE68793 LUSC dataset and identified *CHAF1B* as one of the most important driver gene candidates. Immunohistochemical analysis of 126 LUSC tumor samples and 80 adjacent normal lung tissues showed the marked upregulation of CHAF1B in tumor tissues and the negative association of its expression level with patient survival outcomes. Silencing of *CHAF1B* suppressed LUSC proliferation *in vitro* and LUSC tumor growth *in vivo.* Furthermore, bulk RNA sequencing of *CHAF1B* knockdown cells indicated SET domain containing 7 (*SETD7*) as a significant CHAF1B target gene. In addition, CHAF1B competitively binds to the *SETD7* promoter region and represses its transcription. Altogether, these results imply that CHAF1B plays a vital role in LUSC tumorigenesis and may represent a potential molecular target for this deadly disease.**

Keywords *CHAF1B*; cell cycle; lung squamous cell carcinoma; *SETD7*; WGCNA

Introduction

Lung cancer was the leading cause of cancer-related mortality globally in 2022, with an estimated 2.5 million new cases and 1.76 million deaths worldwide. In China alone, approximately 1.06 million new cases and 733 300 deaths have been recorded in 2022 [1,2]. Lung cancer falls under two major histological types: small-cell lung cancer (SCLC), which represents 15% of lung cancers, and non-small cell lung cancer (NSCLC), which accounts 85% of lung cancers. NSCLC can be further classified into lung adenocarcinoma (LUAD; 40% of NSCLC), lung squamous-cell carcinoma (LUSC; 30%), and large-cell lung carcinoma (LCLC; 15%) [3]. LUSC develops in the proximal region of the lungs and originates from the basal cells of bronchi. This condition is distinguished by its distinct squamous morphology and high genomic tumor mutational burden [4]. Targeted therapies, such as inhibitors of epidermal growth factor receptor and immune checkpoint inhibitors (ICIs), including those targeting programmed cell death 1 and programmed cell death-ligand 1 proteins, have considerably prolonged the overall survival of patients suffering from LUAD [5–7]. However, the effectiveness of ICIs covers only 20% of LUSCs, and no targeted therapy is available because of limited driver genes and biomarkers [8]. Currently, the 5-year survival rate of patients with LUSC is less than 15% [9,10]; therefore, new molecular indicators and treatment targets must be developed for the effective management of LUSC.

The p60 subunit of the chromatin assembly factor 1 (CAF-1) complex, known as the seven-tryptophan-aspartate-repeat-containing protein CAF-1 subunit B (CHAF1B), mediates the interaction between the antisilencing function 1A histone chaperone/histone H3/histone H4 and CHAF1A within the CAF-1 complex [11]. CHAF1B is a central facilitator delivering newly synthesized histones to DNA replication forks for chromatin assembly during the S phase of the cell cycle; and it also regulates nucleotide excision repair following DNA damage [12]. Under physiologic conditions,

Received November 4, 2024; accepted November 14, 2024
Correspondence: Guangbiao Zhou, gbzhou@cicams.ac.cn

CHAF1B plays a critical role in preventing the mislocalization of death domain-associated protein-dependent centromere protein A and chromosomal instability [13]. In addition, CHAF1B acts as an oncoprotein and shows a high expression in solid tumors [14–17] and hematopoietic malignancies [18–20]. In acute myeloid leukemia (AML), the effects of CHAF1B are linked to AML blast self-renewal capacity and their undifferentiated state [11]. CHAF1B functions downstream of miR-3619-5p and circular RNA circ_0026134 in NSCLC [21]. In patients with LUAD, CHAF1B serves as an E3 ubiquitin ligase that induces the degradation of the nuclear receptor corepressor 2, promotes cisplatin resistance [22], enhances cell proliferation, and exhibits an inverse correlation with a poor prognosis [23]. However, the role of CHAF1B in LUSC has rarely been reported.

In this study, we aimed to construct LUSC-related gene networks and identify the central nodes using the Gene Expression Omnibus GSE68793 LUSC data set and weighted gene co-expression network analysis (WGCNA) [24]. The top three enriched pathways in LUSC comprised the cell cycle, DNA replication, and base excision repair pathways, and *CHAF1B* was one of the most considerably altered genes. CHAF1B was highly expressed in LUSC tumor samples and negatively associated with patient prognosis. The knockdown of *CHAF1B* elevated the expression of SET domain containing 7 (*SETD7*) and inhibited LUSC cell proliferation *in vitro* and *in vivo*. This study revealed that CHAF1B may have an important role in carcinogenesis and serve as a potential molecular target for LUSC treatment.

Materials and methods

Patient samples

This study received approval from the Institutional Review Boards of the Cancer Hospital, Chinese Academy of Medical Sciences, and Peking Union Medical College (approval No. NCC2020A190). A minimum of two independent pathologists verified the diagnostic assessment of patients with LUSC. Microarray slides of LUSC tissue (product Nos. HLug-Squ150Sur-02 and HLugS180Su02) were obtained from Shanghai Outdo Biotech, China. Written informed consent was obtained from all patients. Table 1 shows the comprehensive pathological details of these samples.

Cell culture

LUSC (H520, H1703, and H226) and LCLC (H1299) cell lines were obtained from the American Tissue Culture Collection (ATCC, USA) and grown in Dulbecco's modified Eagle medium or Roswell Park Memorial Institute 1640 with 10% fetal bovine serum (Gibco, USA). Cells were cultured in a climate-controlled environment to maintain optimal growth conditions.

Cell viability assay

H520 and H1299 cells were transfected with si*CHAF1B*

Table 1 Clinicopathological characteristics and expression of CHAF1B in LUSC

Characteristics	Total, *n* (%)	CHAF1B-high, *n* (%)	CHAF1B-low, *n* (%)	*P* values
Total	126	63 (50.0%)	63 (50.0%)	
Gender				0.05
Male	119/126 (94.4%)	57 (47.9%)	62 (52.1%)	
Female	7/126 (5.60%)	6 (85.7%)	1 (14.3%)	
Age, year				0.37
⩽ 60	55/126 (43.7%)	30 (54.5%)	25 (45.5%)	
> 60	71/126 (56.3%)	33 (46.5%)	38 (53.5%)	
Site				0.87
Central	52/126 (41.3%)	27 (51.9%)	25 (48.1%)	
Peripheral	11/126 (8.70%)	6 (54.5%)	5 (45.5%)	
n.d.	63/126 (50.0%)	30 (47.6%)	33 (52.4%)	
TNM_stage				0.03
I	37/126 (29.4%)	17 (45.9%)	20 (54.1%)	
II	36/126 (28.6%)	11 (30.6%)	25 (69.4%)	
III	23/126 (18.2%)	15 (65.2%)	8 (34.8%)	
n.d.	30/126 (23.8%)	18 (60.0%)	12 (40.0%)	

Abbreviations: CHAF1B, chromatin assembly factor 1 subunit B; T, tumor; N, node; M, metastasis; n.d., not determined.

or a negative control siRNA (siNC) (GenePharma) using Lipofectamine 3000 transfection reagent. Table S1 lists the corresponding the siRNA sequences. The cells were harvested, reseeded at an appropriate density, and cultured for various time intervals. Cell proliferation was assessed using a 1:10 dilution of Cell Counting Kit-8 (CCK-8) solution in the culture medium, with a subsequent 1 h incubation. Cell viability was assessed through measurement of the optical density (OD) of each well at 450 nm. Relative cell viability was determined using the formula: $(OD_{exp} - OD_{blank})/ (OD_{control} - OD_{blank}) \times 100\%$, where OD_{exp} and $OD_{control}$ denote the absorbance values of the experimentally treated and control cells, respectively.

Colony formation assay

H520 and H1299 cells were transfected with siNC or si*CHAF1B* for 48 h using Lipofectamine 3000 reagent. After harvest, the cells were plated at an appropriate density. After 7–14 days, the cells were fixed in methanol, washed twice with phosphate buffered saline (PBS), and stained with 0.005% crystal violet (Sigma-Aldrich, USA). Colonies with more than 50 cells were identified and quantified.

Cell cycle

H520, H1703, H226, and H1299 cell lines were transfected with siNC or si*CHAF1B* using Lipofectamine 3000 reagent for 72 h. After transfection, the cells were fixed in 70% ethanol at −20 °C, washed twice with PBS, and treated with ribonuclease A. Subsequently, the cells were stained with propidium iodide for DNA labeling. Cell distribution across different cell cycle phases was assessed using a FACSCalibur flow cytometer (Becton Dickinson, USA).

RNA isolation and quantitative real-time polymerase chain reaction (qRT-PCR)

RNA was isolated using TRIzol (Invitrogen, USA) and reverse transcribed into cDNA using HiFiScript RT SuperMix (Vazyme, China). qRT-PCR was conducted using the SYBR qPCR Master Mix (Vazyme, China) and the reference gene *GAPDH* as a control. Gene expression was calculated using the $2^{-\Delta\Delta CT}$ method. Table S1 provides the primer sequences.

Immunoprecipitation (IP) and Western blot

The cells were lysed on ice using an IP buffer and high-speed centrifugation, and the supernatants were incubated with antibodies (Table S1) overnight. Protein A/G agarose was added, and the beads were washed and boiled in the loading buffer. The input and IP samples were subjected to Western blot analysis. Table S1 lists the specific antibodies used.

Lentivirus-mediated transfection

To construct the sh*CHAF1B*-expressing vector, we inserted sh*CHAF1B* sequences into the pSIH1-H1-Puro shRNA vector backbone, which was then co-transfected with psPAX2 and pMD2.G into HEK293T cells. Then, lentiviral supernatants were collected from the HEK293T cells. *CHAF1B*-stable knockdown cells were established by infecting H520 and H1299 cells with lentiviral supernatants in the presence of polybrene (Yeasen Biotechnology, China), followed by puromycin selection. Table S1 lists the shRNA primers used.

Immunohistochemical analysis

Deparaffinization of 5 μm-thick paraffin-embedded LUSC tissue sections with xylene was conducted, followed by rehydration in a series of alcohols. The tissue sections were subjected to a heat-induced epitope retrieval step in a citrate buffer solution and blocked with 5% bovine serum albumin. Next, the sections were incubated with primary antibodies overnight, followed by a 90 min incubation with horseradish peroxidase-conjugated secondary antibodies (Table S1). 3,3′-Diaminobenzidine was used as a chromogenic reagent. The immunoreactivity score (IRS) was determined through separate scoring of the staining intensity (SI, 0–3 points) and the proportion of positively stained cells (RP, 0–4 points) in the immunohistochemical sections. In addition, composite IRS (0–12 points) was obtained using the formula SI × RP.

Chromatin immunoprecipitation

Cells cultured in a 10 cm dish were crosslinked with 1% formaldehyde, and the reaction was neutralized with glycine. Sonication was performed to fragment the chromatin associated with proteins into smaller pieces via. Protein–DNA complexes were immunoprecipitated using an anti-CHAF1B antibody, with normal rabbit IgG serving as the negative control. Table S1 lists the antibodies used in this study. Next, Protein A + G Agarose/Salmon Sperm DNA was mixed into the solution at 4 °C. After IP, DNA was decrosslinked, and proteins were removed via digestion using proteinase K. DNA was subsequently collected and prepared for PCR. Table S1 contains the primer sequences used in this work.

Animal studies

The animal experiments were approved by the relevant

ethics committee of the Chinese Academy of Medical Sciences Cancer Institute and Hospital (NCC2020A190). Five-week-old, female nonobese diabetic/ShiLtJGpt-Prkdc^{em26Cd52}Il2rg^{em26Cd22}/Gpt mice (NCG; GemPharmatech, China) were maintained in a specific pathogen-free environment. H520-NC and H520-sh*CHAF1B* cells (2×10^6) were subcutaneously inoculated into the mice ($n = 7$ per group). Tumor size measurement was conducted every four days, with volumes calculated as $1/2 \times \text{length} \times \text{width}^2$. Once tumors reached 2 cm or the mice displayed symptoms of morbidity, the tumors were excised, photographed, and subjected to subsequent experimental analyses.

Online data availability

The gene expression dataset for LUSC (GSE68793) was obtained from the website of NCBI Series GSE68793. The TIMER database was used in the evaluation of expression of *CHAF1B* in tissues. Survival prognoses were analyzed using the Kaplan–Meier plotter, and the enriched pathways correlated with *CHAF1B* were assessed using the LinkedOmics database.

Statistical analysis

Each experiment was conducted in triplicate at least. Mono-methyltransferase data are expressed as mean values ± standard deviation (SD). Statistical evaluations were conducted using SPSS (version 23.0) and GraphPad Prism (version 8.0) software. The statistical methods applied to the data included two-tailed Student's *t*, chi-square, and log-rank tests. $P < 0.05$ was considered statistically significant.

Results

Identification of *CHAF1B* as a key gene in LUSC

We analyzed the altered genes in the LUSC public data set (GSE68793), which comprised 134 tumor samples. The top 5000 altered genes were used to create joint-expression modules via WGCNA [24,25], and 24 modules were identified based on a single-step approach for module construction and identification (Fig. S1A). Fig. S1B shows the results of module–trait association analysis. Kyoto Encyclopedia of Genes and Genomes pathway analysis was performed on the most significant module (black) to determine the top three most enriched pathways, namely, the cell cycle, DNA replication, and base excision repair pathways (Fig. 1A). To better identify the pivotal genes in this module, we evaluated protein–protein interactions and depicted them using Cytoscape with the MCODE plugin [26,27]. In general, 50 significant hub genes in the circle were identified as crucial targets among differentially expressed genes (DEGs) in LUSC (Fig. 1B). Comparison of these hub genes with the 648 cell cycle pathway genes [28] identified 27 candidates, including *CDC45*, *TTK*, and *CHAF1B* (Fig. 1C). Among these genes, *CDC45* [29] and *TTK* [30] regulate the proliferation of LUSC and LUAD (Table S2). However, the significance of *CHAF1B*, an important cell cycle regulatory protein [31], has been understudied in LUSC. Therefore, *CHAF1B* was selected for further investigation.

The *CHAF1B* levels in cancerous and adjacent healthy tissue were assessed using the TIMER database [32–34], and the findings indicate the marked increase in the *CHAF1B* mRNA level in tumor samples of bladder urothelial carcinoma (BLCA), breast invasive carcinoma (BRCA), cholangiocarcinoma (CHOL), colon adenocarcinoma (COAD), esophageal carcinoma (ESCC), head-and-neck carcinoma (HNSC), liver hepatocellular carcinoma (LIHC), LUAD, LUSC, prostate adenocarcinoma (PRAD), rectal adenocarcinoma (READ), stomach adenocarcinoma (STAD), thyroid cancer (THCA), and uterine corpus endometrial cancinoma (UCEC), compared with their counterpart normal tissue (Fig. 1D). Kaplan–Meier plotter database was used to assess the association between *CHAF1B* mRNA expression and overall survival of patients suffering from NSCLC [35,36]. We discovered that elevated *CHAF1B* expression was linked to poor prognosis of patients with NSCLC (Fig. 1E).

Validation of CHAF1B in LUSC tissue samples

To further validate the significance of CHAF1B in LUSC, we analyzed 126 LUSC samples and 80 adjacent normal lung tissues from tissue microarrays via immunohistochemistry. Among these patients, 119 (94.4%) were male, 7 (5.56%) were female, 55 (43.7%) were aged ⩽ 60 years, and 71 (53.6%) were > 60 years of age (Table 1). However, no data were available on the smoking status of these 126 patients, although most male patients with LUSC are smokers. CHAF1B was mainly localized in the nuclear compartment but was rarely detected in the cytoplasmic fraction (Fig. 2A and 2B). A higher CHAF1B IRS was observed in tumor tissues than in adjacent normal lung tissues (Fig. 2C). In tumor tissues, CHAF1B expression fell under four categories based on SI: negative, weak, moderate, and strong (Fig. 2B). The median IRS value served as a threshold, with IRS values above it being classified as high, and those at or below classified as low. CHAF1B expression exhibited an inverse association with overall survival (Fig. 2D), which is consistent with the findings of the LUSC data set analysis presented in Fig. 1E. These data suggest that CHAF1B serves as an oncoprotein in LUSC progression.

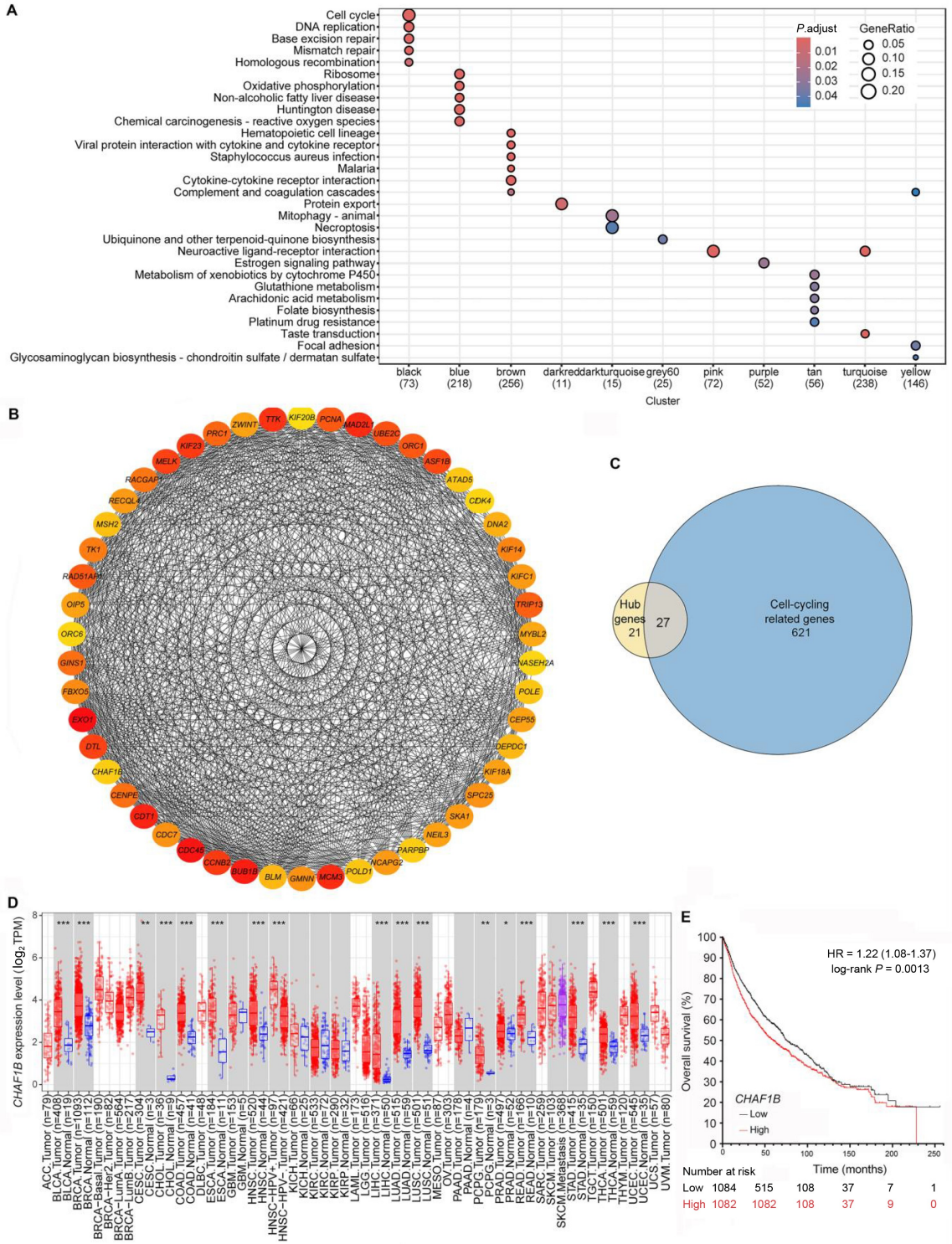

Fig. 1 Identification of *CHAF1B* as a key gene in NSCLC. (A) Annotation of GSE68793 gene modules identified via WGCNA. The 11 modules were labeled by color. (B, C) The 50 DEGs in the most significant (black) module (B) were screened for their involvement in cell cycle regulation (C), and 27 genes were identified. (D) *CHAF1B* expression in various cancer types; it was analyzed using the TIMER database containing TCGA data sets. (E) Correlation between *CHAF1B* expression level and overall survival of patients with NSCLC.

CHAF1B promotes LUSC cell proliferation

We explored the effects of CHAF1B on LUSC proliferation through transfection of sh*CHAF1B* siRNA or lentivirus into H520, H1703, H226, and H1299 cells, followed by cell proliferation analysis using CCK8 assay.

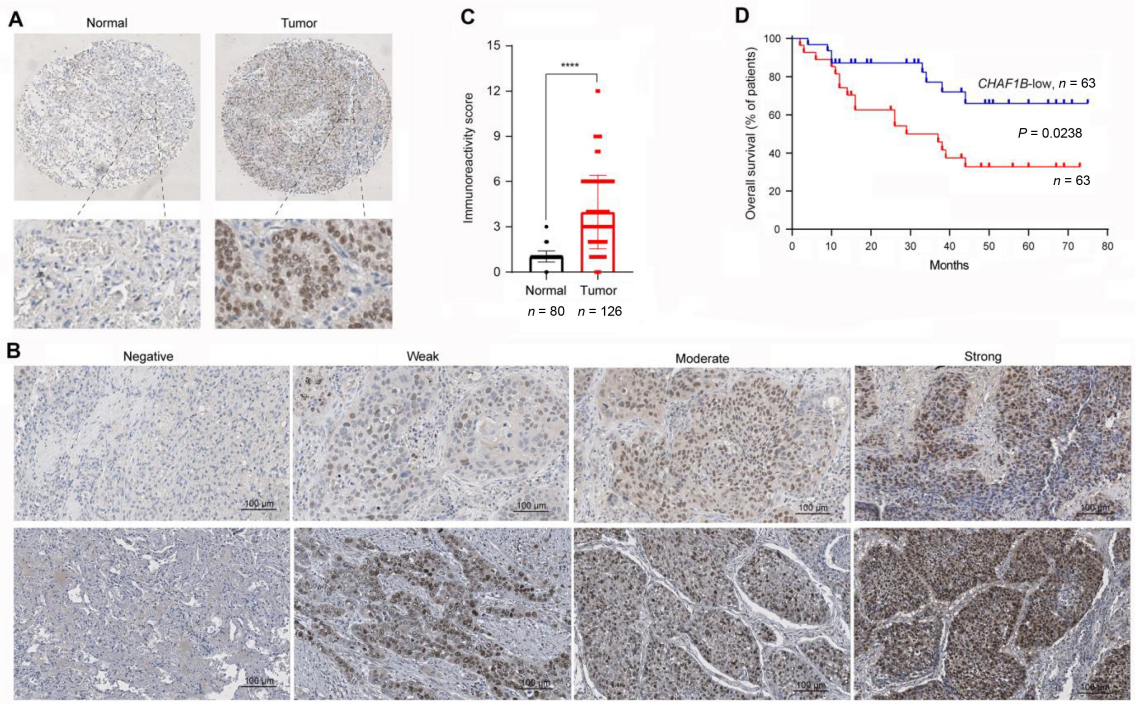

Fig. 2 CHAF1B showed an overexpression in LUSC tumor tissues and a negative association with overall survival. (A, B) Representative immunohistochemistry staining images of CHAF1B (A). SI was classified into four categories: negative, weak, moderate, and strong (B). (C) IRS of CHAF1B in LUSC tumor tissues (n = 126) and adjacent normal lung tissues (n = 80). Data are shown as mean ± SD. P value was determined through Wilcoxon rank-sum test. ****, $P < 0.0001$. (D) Overall survival of the 126 patients with LUSC. P value was determined via log-rank test.

CHAF1B knockdown considerably suppressed the proliferation of these cell lines (Figs. 3A–3D, S2A, and S2B). Correspondingly, *CHAF1B* overexpression promoted the growth of H1703 and H226 cells after transfection with *CHAF1B* plasmids (Fig. 3E and 3F). Colony formation experiments demonstrated the reduced colony formation in H520 and H1299 cells after *CHAF1B* knockdown (Fig. 3G and 3H). The effect of *CHAF1B* on the cell cycle was further determined, and we observed that si*CHAF1B*-transfected cells were arrested in the S phase (Fig. 3I). These findings suggest the crucial role of *CHAF1B* in LUSC growth.

SETD7 serves as a potential downstream target of CHAF1B

To gain insights into the downstream targets of CHAF1B in promoting LUSC, we conducted bulk RNA sequencing on siNC- and si*CHAF1B*-transfected H520 and H1299 cells and evaluated the genes with altered expression (increased and decreased) (Fig. S3A). Compared with the siNC groups, 109 DEGs were found in si*CHAF1B*-transfected H1299 and H520 cells (Fig. 4A). Notably, eight DEGs, including the *SETD7* (also termed *SET7/9*, and *KMT7*), hyaluronan binding protein 4 (*HABP4*), tropomyosin 4 (*TPM4*), caspase 7 (*CASP7*), dehydrogenase/reductase 2 (*DHRS2*), regulator of solute carriers 1 (*RSC1A1*), neuroplastin (*NPTN*), and heme oxygenase 1 (*HMOX1*), were selected for further analysis because their fold changes ($\log_2$) were > 1 or < −1 in both cell lines (Fig. 4B). To assess the mRNA levels of these genes after *CHAF1B* knockdown in H520 and H1299 cells, we conducted qRT-PCR, and the findings reveal the significant upregulation of *SETD7* in H520 and H1299 cells (Fig. 4C).

SETD7 is a histone lysine methyltransferase containing seven structural domains responsible for the methylation of catalytic SETs [37]. SETD7 mediates KRAS methylation and subsequent degradation and attenuates the RAS/mitogen-activated protein kinase/extracellular-signal-regulated kinase signaling cascade; thus, it acts as a tumor suppressor in NSCLC [38]. We hypothesized that CHAF1B promotes LUSC progression by inhibiting the tumor suppressor *SETD7*. To test this possibility, we performed Western blot analysis, and the findings reveal the elevated SETD7 levels following CHAF1B knockdown (Figs. 4D and S3B). By contrast, CHAF1B overexpression inhibited SETD7 expression in H1703 cells (Fig. 4E). Notably, CHAF1B protein levels exhibited no substantial change after SETD7 knockdown, which indicates that *SETD7* did not regulate CHAF1B expression (Fig. 4F). Using the NSCLC data sets in Kaplan–Meier plotter [35,36], we demonstrated the linkage of elevated levels of *SETD7* to improved patient

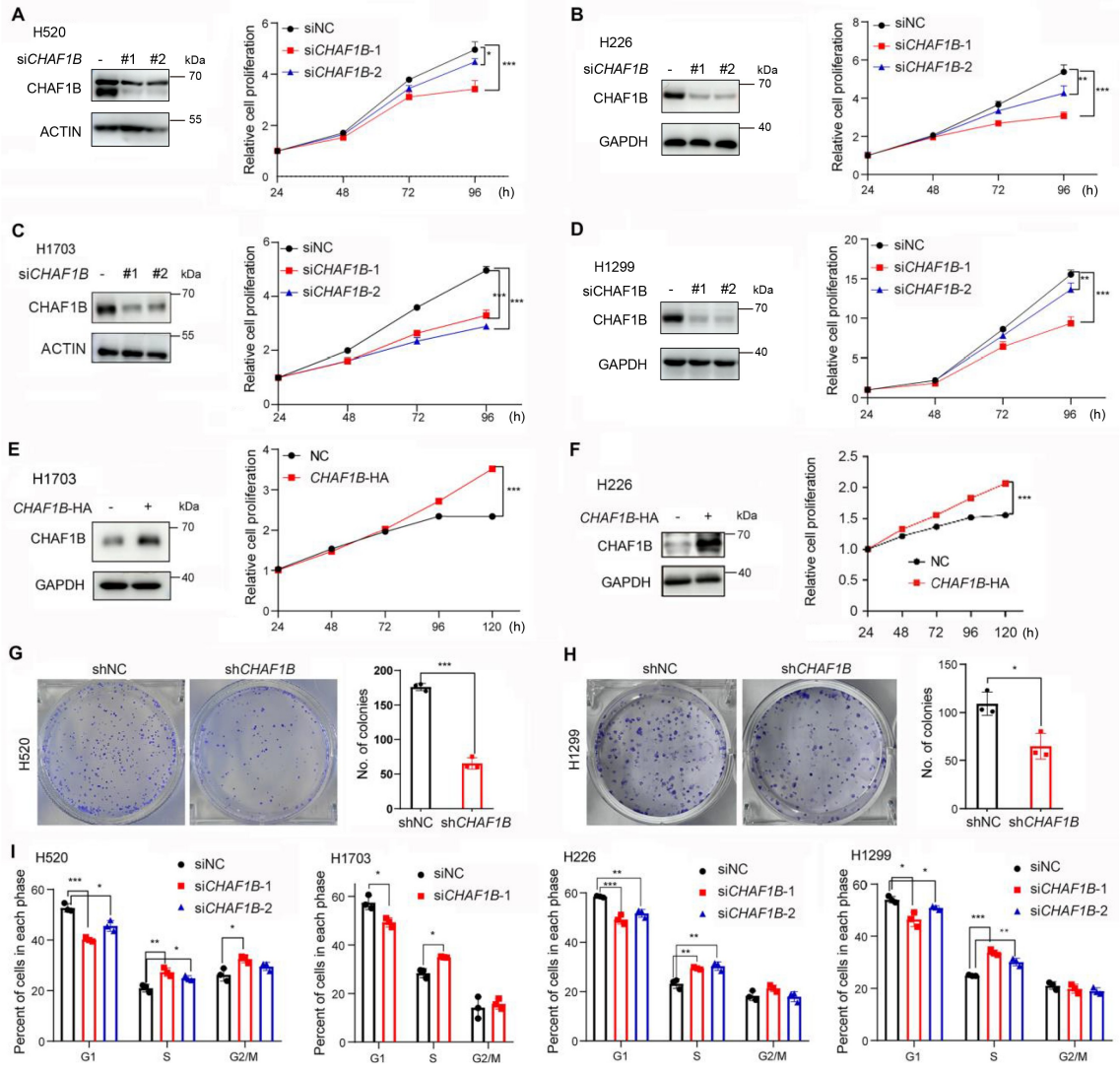

Fig. 3 CHAF1B promotes LUSC cell proliferation *in vitro*. (A–D) Knockdown of *CHAF1B* suppressed the proliferation of H520 (A), H226 (B), H1703 (C), and H1299 (D) cells. The cells were transfected with siRNA for 48 h, protein expression level was determined through Western blot, and cell proliferation was assessed via CCK-8 assay. (E, F) Effects of *CHAF1B*-overexpression on the proliferation of H1703 (E) and H226 (F) cells were tested by CCK-8 assay. (G, H) Colony formation of H520 (G) and H1299 (H) cells was evaluated after stable knockdown of *CHAF1B*. (I) Cell cycle distribution of *CHAF1B*-silenced cells. Data are shown as mean ± SD. *P* values were determined using Student's *t* test. *, $P < 0.05$; **, $P < 0.01$; and ***, $P < 0.001$.

outcomes (Fig. 4G). In addition, cell viability was increased during *SETD7* knockdown, and co-knockdown of *SETD7* and *CHAF1B* rescued H1299 and H520 cell proliferation compared with *CHAF1B*-silenced cells (Fig. 4H and 4I). These data suggest a critical role for SETD7 in the CHAF1B pathway. The co-IP assay revealed no direct association between CHAF1B and SETD7 at the protein level (Fig. 4J). Chromatin IP experiments using PCR primer pairs for segments of the *SETD7* promoter region (Table S1) unveiled that CHAF1B bound *SETD7* at the regions of primer pairs 3, 4, 5, 8, 16, and 17 (Fig. 4K). These results prove the function of CHAF1B as a cotranscriptional regulator of *SETD7* expression at the transcription level.

CHAF1B is required for tumor growth in mice

To evaluate the effect of CHAF1B on tumorigenicity *in vivo*, we subcutaneously injected NCG mice with control or *CHAF1B* knockdown H520 cells. The findings demonstrate that stable depletion of CHAF1B markedly inhibited tumor growth compared with that in the siNC group (Fig. 5A). Mice in the H520-shCHAF1B group displayed substantially lower tumor volumes and weights than those in the H520-shNC group (Fig. 5B and 5C). Western blot analysis was conducted to detect the CHAF1B and SETD7 protein levels in harvested tumor tissues, and the results demonstrate the significant upregulation of SETD7 upon *CHAF1B* knockdown

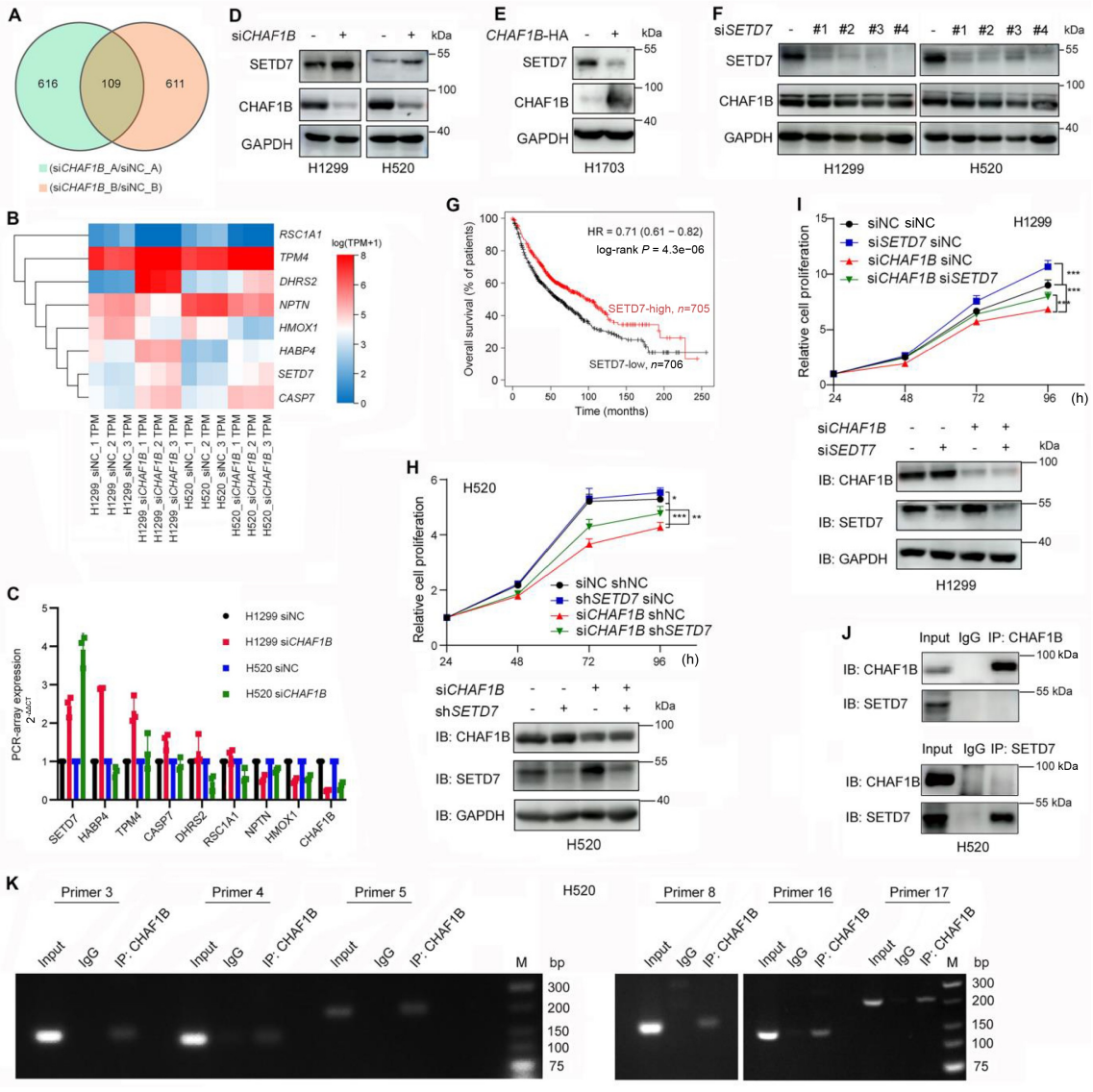

Fig. 4 *SETD7* may be downstream of CHAF1B. (A) A total of 109 DEGs found in si*CHAF1B*-1-transfected H1299 and H520 cells. (B) Heatmap of the eight DEGs found in si*CHAF1B*-1-transfected H1299 and H520 cells. (C) qRT-PCR analysis of the DEGs in H1299 and H520 cells transfected with siNC or si*CHAF1B*-1. (D) Protein level of SETD7 after transient knockdown of *CHAF1B* using si*CHAF1B*-1. (E) SETD7 protein level after transient overexpression of *CHAF1B*. (F) CHAF1B expression level after transient knockdown of *SETD7*. (G) *SETD7* expression in lung cancer showed a positive association with patient survival outcomes as analyzed by Kaplan–Meier plotter. (H, I) Cell proliferation was evaluated via CCK-8 assays involving H1299 (H) and H520 cells (I) after transfection of si*CHAF1B*-1 and/or sh*SETD7*. (J) Interaction of CHAF1B and SETD7 determined using co-IP assay using anti-CHAF1B and anti-SETD7 antibodies in H520 cells. (K) Potential CHAF1B binding sites in the *SETD7* promoter were evaluated via PCR. M, DNA marker. Data are shown as mean ± SD. *P* values in H and I were determined through Student's *t* test. *, $P < 0.05$; ***, $P < 0.001$.

(Fig. 5D). Immunohistochemical analysis revealed the downregulation of CHAF1B and Ki67 in H520-sh*CHAF1B* mice compared with those in the H520-shNC group (Fig. 5E). These findings imply the important role of in LUSC tumor development *in vivo*.

Discussion

CHAF1B was initially identified as part of the CAF-1 complex, which is a conserved three-component complex comprising RBBP4, CHAF1A, and CHAF1B; it facilitates histone H3–H4 deposition during the S phase of the cell cycle [39,40]. Physiologically, CHAF1B assembles chromatin during the S phase of DNA synthesis in the cell cycle [12]. During embryonic development, enhanced *CHAF1B* expression may contribute to a high cellular replication rate [41]. CHAF1B expression shows a positive association with the proliferation marker Ki67 in several solid tumors [14]. In AML, CHAF1B overexpression promotes leukemia,

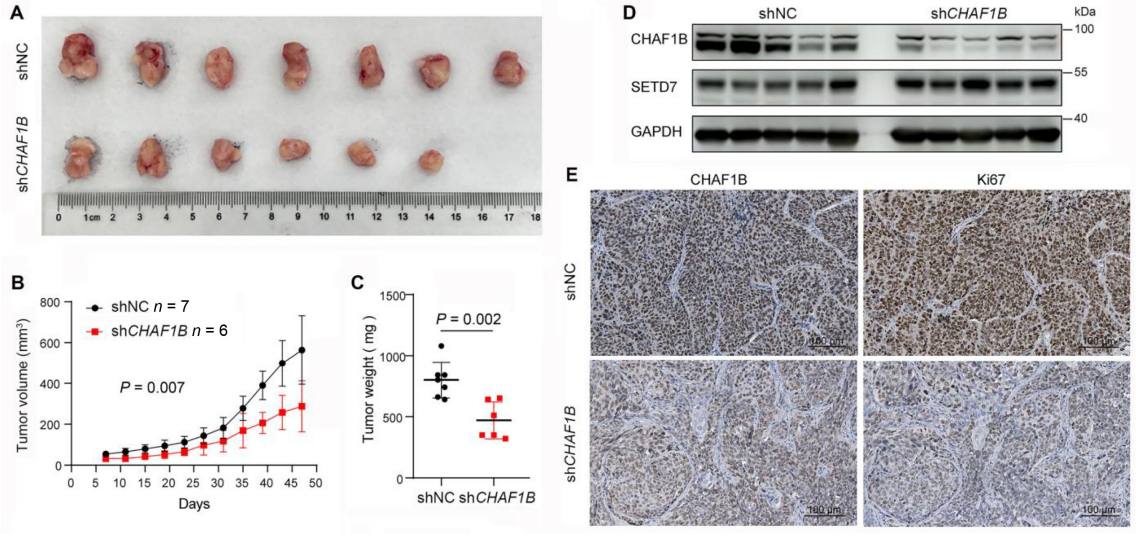

Fig. 5 Effects of CHAF1B on lung tumorigenesis *in vivo*. (A) Photographs of tumors in the shNC and sh*CHAF1B* groups. (B) Tumor growth curves of the shNC and sh*CHAF1B* groups. (C) Final tumor weight of the shNC and sh*CHAF1B* groups. (D) Western blot analysis of CHAF1B and SETD7 expressions in tumors. (E) Representative immunohistochemical images revealing the protein expressions of CHAF1B and Ki67 in tumor tissues from different groups. Data are shown as mean ± SD. *P* values in (B) and (C) were determined by Student's *t* test.

whereas the suppression of CHAF1B activity substantially inhibits leukemogenesis *in vivo* without impairing normal hematopoiesis [11]. In addition, *CHAF1B* silencing results in cell accumulation in the S phase during DNA replication due to chromatin assembly defects, which leads to programmed cell death [41]. However, the role of CHAF1B in LUSC remains unclear. This study showed the overexpression of *CHAF1B* in LUSC and the negative correlation of its expression level with the clinical outcomes of patients with LUSC. Stable and transient knockdown of *CHAF1B* notably suppressed LUSC cell proliferation and arrested cell cycle in the S phase. Consistently, *in vivo* experiments confirmed that the stable knockdown of *CHAF1B* in LUSC cells tremendously inhibited tumor growth. These data indicate the role of CHAF1B as an oncoprotein in LUSC.

CHAF1B is a key epigenetic regulator at the transcriptional level and associated with cell state and self-renewal. This molecule can bind to various gene enhancers and promoters, such as CCAAT enhancer binding protein alpha, which leads to the inhibition of these genes through the displacement of transcription factors [11]. To identify the target genes of CHAF1B in LUSC, we conducted bulk RNA-seq in *CHAF1B* silenced cells and observed that the expressions of eight candidate genes were markedly altered, with *SETD7* being the most considerably upregulated gene. We further confirmed that CHAF1B bound *SETD7* at its promoter and suppressed its expression, and knockdown of *CHAF1B* resulted in extensive upregulation of *SETD7*. SETD7 stabilizes the tumor suppressor p53 and facilitates its nuclear translocation to augment p53 transactivation through its lysine methylation at residue 372 [42]. These data suggest that *CHAF1B* promotes LUSC tumorigenesis, likely through the downregulation of *SETD7* expression, and thus inhibits the SETD7-mediated p53 cascade.

SETD7 contains 366 amino acids and comprises three motifs in the membrane occupation–recognition nexus. This mono-methyltransferase can modify various substrates, including p53, KRAS, and Rb1 [37,38,43,44]. *SETD7* is involved in several pathological processes, including abnormal development, aberrant tissue regeneration, and neurodegeneration. It functions as a tumor promoter in hepatocellular carcinoma [45] and displays a direct association with drug resistance and cancer relapse. However, *SETD7* is also a tumor suppressor in *KRAS*-driven NSCLC [38]. Herein, we showed that *SETD7* knockdown contributed to enhanced NSCLC cell proliferation and that a high *SETD7* expression correlated with good survival outcomes in patients. This finding indicates that *SETD7* may be a tumor suppressor in LUSC. To date, only a few molecules, such as long non-coding RNAs, including small nucleolar RNA host gene 15 (*SNHG15*) and miR-153-3p, have been shown to regulate *SETD7* expression [46]. Here, we report for the first time that CHAF1B suppresses *SETD7* expression by binding to its promoter and inhibiting its transcription, and these findings provide the potential mechanisms for controlling SETD7 expression.

In conclusion, CHAF1B expression is elevated in patients with LUSC and inversely correlates with survival outcomes. Ectopic CHAF1B expression promoted LUSC proliferation *in vitro* and in animal models. RNA-seq revealed that *SETD7* is a downstream target of CHA1B, and CHAF1B suppressed *SETD7* mRNA levels, possibly

through competitive binding to *SETD7*'s promoter site and interference with transcription factor promoter occupancy. This study suggests that CHAF1B may serve as an oncoprotein in LUSC tumorigenesis and that CHAF1B-targeted therapy may provide a potential therapeutic approach for LUSC.

Acknowledgements

This work was supported by the National Key Research and Development Program of China (Nos. 2022YFA1103900 and 2020YFA0803300), CAMS Initiative for Innovative Medicine (Nos. 2021-1-I2M-012, 2021-I2M-1-014, 2022-I2M-2-001, 2021-I2M-1-021, and 2022-I2M-1-009), the Non-Profit Central Research Institute Fund of CAMS (Nos. 2022-RC310-05 and 2021-RC310-003), and the National Natural Science Foundation of China (Nos. 82372944, 82073092, and 82273076).

Compliance with ethics guidelines

Conflicts of interest Zhuo Zheng, Yongfang Lin, Hua Guo, Zheng Liu, Xiaoliang Jie, Guizhen Wang, and Guangbiao Zhou declare that they have no conflict of interest.

The study was approved by the research ethics committee of the Cancer Hospital, Chinese Academy of Medical Sciences and performed in accordance with the ethical standards laid down in the 1964 *Declaration of Helsinki* and its later amendments or comparable ethical standards. Additional informed consent was obtained from all patients, whose identifying information is included in this article.

Electronic Supplementary Material Supplementary material is available in the online version of this article at https://doi.org/10.1007/s11684-024-1122-2 and is accessible for authorized users.

References

1. Bray F, Laversanne M, Sung H, Ferlay J, Siegel RL, Soerjomataram I, Jemal A. Global cancer statistics 2022: GLOBOCAN estimates of incidence and mortality worldwide for 36 cancers in 185 countries. CA Cancer J Clin 2024; 74(3): 229–263
2. Zheng RS, Chen R, Han BF, Wang SM, Li L, Sun KX, Zeng HM, Wei WW, He J. Cancer incidence and mortality in China, 2022. Chinese Journal of Oncology (Zhonghua Zhongliu Zazhi) 2024; 46(3): 221–231 (in Chinese)
3. Thai AA, Solomon BJ, Sequist LV, Gainor JF, Heist RS. Lung cancer. Lancet 2021; 398(10299): 535–554
4. Pan Y, Han H, Labbe KE, Zhang H, Wong KK. Recent advances in preclinical models for lung squamous cell carcinoma. Oncogene 2021; 40(16): 2817–2829
5. Zhong J, Bai H, Wang Z, Duan J, Zhuang W, Wang D, Wan R, Xu J, Fei K, Ma Z, Zhang X, Wang J. Treatment of advanced non-small cell lung cancer with driver mutations: current applications and future directions. Front Med 2023; 17(1): 18–42
6. Garon EB, Rizvi NA, Hui R, Leighl N, Balmanoukian AS, Eder JP, Patnaik A, Aggarwal C, Gubens M, Horn L, Carcereny E, Ahn MJ, Felip E, Lee JS, Hellmann MD, Hamid O, Goldman JW, Soria JC, Dolled-Filhart M, Rutledge RZ, Zhang J, Lunceford JK, Rangwala R, Lubiniecki GM, Roach C, Emancipator K, Gandhi L. Pembrolizumab for the treatment of non-small-cell lung cancer. N Engl J Med 2015; 372(21): 2018–2028
7. Horn L, Spigel DR, Vokes EE, Holgado E, Ready N, Steins M, Poddubskaya E, Borghaei H, Felip E, Paz-Ares L, Pluzanski A, Reckamp KL, Burgio MA, Kohlhäeufl M, Waterhouse D, Barlesi F, Antonia S, Arrieta O, Fayette J, Crinò L, Rizvi N, Reck M, Hellmann MD, Geese WJ, Li A, Blackwood-Chirchir A, Healey D, Brahmer J, Eberhardt WEE. Nivolumab versus docetaxel in previously treated patients with advanced non-small-cell lung cancer: two-year outcomes from two randomized, open-label, phase III trials (CheckMate 017 and CheckMate 057). J Clin Oncol 2017; 35(35): 3924–3933
8. Novello S, Kowalski DM, Luft A, Gümüş M, Vicente D, Mazières J, Rodríguez-Cid J, Tafreshi A, Cheng Y, Lee KH, Golf A, Sugawara S, Robinson AG, Halmos B, Jensen E, Schwarzenberger P, Pietanza MC, Paz-Ares L. Pembrolizumab plus chemotherapy in squamous non-small-cell lung cancer: 5-year update of the phase III KEYNOTE-407 study. J Clin Oncol 2023; 41(11): 1999–2006
9. Sung H, Ferlay J, Siegel RL, Laversanne M, Soerjomataram I, Jemal A, Bray F. Global cancer statistics 2020: GLOBOCAN estimates of incidence and mortality worldwide for 36 cancers in 185 countries. CA Cancer J Clin 2021; 71(3): 209–249
10. Duma N, Santana-Davila R, Molina JR. Non-small cell lung cancer: epidemiology, screening, diagnosis, and treatment. Mayo Clin Proc 2019; 94(8): 1623–1640
11. Volk A, Liang K, Suraneni P, Li X, Zhao J, Bulic M, Marshall S, Pulakanti K, Malinge S, Taub J, Ge Y, Rao S, Bartom E, Shilatifard A, Crispino JD. A CHAF1B-dependent molecular switch in hematopoiesis and leukemia pathogenesis. Cancer Cell 2018; 34(5): 707–723.e7
12. Volk A, Crispino JD. The role of the chromatin assembly complex (CAF-1) and its p60 subunit (CHAF1b) in homeostasis and disease. Biochim Biophys Acta 2015; 1849(8): 979–86
13. Shrestha RL, Balachandra V, Kim JH, Rossi A, Vadlamani P, Sethi SC, Ozbun L, Lin S, Cheng KCC, Chari R, Karpova TS, Pegoraro G, Foltz DR, Caplen NJ, Basrai MA. The histone H3/H4 chaperone CHAF1B prevents the mislocalization of CENP-A for chromosomal stability. J Cell Sci 2023; 136(10): jcs260944
14. Polo SE, Theocharis SE, Grandin L, Gambotti L, Antoni G, Savignoni A, Asselain B, Patsouris E, Almouzni G. Clinical significance and prognostic value of chromatin assembly factor-1 overexpression in human solid tumours. Histopathology 2010; 57(5): 716–724
15. Staibano S, Mascolo M, Mancini FP, Kisslinger A, Salvatore G, Di Benedetto M, Chieffi P, Altieri V, Prezioso D, Ilardi G, De Rosa G, Tramontano D. Overexpression of chromatin assembly factor-1 (CAF-1) p60 is predictive of adverse behaviour of prostatic cancer. Histopathology 2009; 54(5): 580–589
16. Peng X, Fu H, Yin J, Zhao Q. CHAF1B knockdown blocks migration in a hepatocellular carcinoma model. Oncol Rep 2018; 40(1): 405–413
17. Di M, Wang M, Miao J, Chen B, Huang H, Lin C, Jian Y, Li Y,

Ouyang Y, Chen X, Wang L, Zhao C. CHAF1B induces radioresistance by promoting DNA damage repair in nasopharyngeal carcinoma. Biomed Pharmacother 2020; 123: 109748
18. Saleiro D, Kosciuczuk EM, Fischietti M, Perez RE, Yang GS, Eckerdt F, Beauchamp EM, Hou Y, Wang Q, Weinberg RS, Fish EN, Yue F, Hoffman R, Platanias LC. Targeting CHAF1B enhances IFN activity against myeloproliferative neoplasm cells. Cancer Res Commun 2023; 3(5): 943–51
19. Li Q, Zhang X, Zhang Z. CHAF1B overexpression: a brake for the differentiation of leukemia cells. Cancer cell 2018; 34(5): 693–4
20. Dean ST, Ishikawa C, Zhu X, Walulik S, Nixon T, Jordan JK, Henderson S, Wyder M, Salomonis N, Wunderlich M, Greis KD, Starczynowski DT, Volk AG. Repression of TRIM13 by chromatin assembly factor CHAF1B is critical for AML development. Blood Adv 2023; 7(17): 4822–37
21. Ge L, Tan W, Li G, Gong N, Zhou L. Circ_0026134 promotes NSCLC progression by the miR-3619–5p/CHAF1B axis. Thorac Cancer 2022; 13(4): 582–92
22. Gong L, Hu Y, He D, Zhu Y, Xiang L, Xiao M, Bao Y, Liu X, Zeng Q, Liu J, Zhou M, Zhou Y, Cheng Y, Zhang Y, Deng L, Zhu R, Lan H, Cao K. Ubiquitin ligase CHAF1B induces cisplatin resistance in lung adenocarcinoma by promoting NCOR2 degradation. Cancer Cell Int 2020; 20: 194
23. Duan Y, Liu T, Li S, Huang M, Li X, Zhao H, Li J. CHAF1B promotes proliferation and reduces apoptosis in 95-D lung cancer cells and predicts a poor prognosis in non-small cell lung cancer. Oncol Rep 2019; 41(4): 2518–2528
24. Langfelder P, Horvath S. WGCNA: an R package for weighted correlation network analysis. BMC Bioinformatics 2008; 9: 559
25. Langfelder P, Horvath S. Fast R functions for robust correlations and hierarchical clustering. J Stat Softw 2012; 46(11): i11
26. Shannon P, Markiel A, Ozier O, Baliga NS, Wang JT, Ramage D, Amin N, Schwikowski B, Ideker T. Cytoscape: a software environment for integrated models of biomolecular interaction networks. Genome Res 2003; 13(11): 2498–504
27. Bader GD, Hogue CW. An automated method for finding molecular complexes in large protein interaction networks. BMC bioinformatics 2003; 4: 2
28. Ben-Porath I, Thomson MW, Carey VJ, Ge R, Bell GW, Regev A, Weinberg RA. An embryonic stem cell-like gene expression signature in poorly differentiated aggressive human tumors. Nat Genet 2008; 40(5): 499–507
29. Huang J, Li Y, Lu Z, Che Y, Sun S, Mao S, Lei Y, Zang R, Li N, Zheng S, Liu C, Wang X, Sun N, He J. Analysis of functional hub genes identifies CDC45 as an oncogene in non-small cell lung cancer-a short report. Cell Oncol (Dordr) 2019; 42(4): 571–578
30. Chen X, Yu C, Gao J, Zhu H, Cui B, Zhang T, Zhou Y, Liu Q, He H, Xiao R, Huang R, Xie H, Gao D, Zhou H. A novel USP9X substrate TTK contributes to tumorigenesis in non-small-cell lung cancer. Theranostics 2018; 8(9): 2348–60
31. Rouillon C, Eckhardt BV, Kollenstart L, Gruss F, Verkennis AEE, Rondeel I, Krijger PHL, Ricci G, Biran A, van Laar T, Delvaux de Fenffe CM, Luppens G, Albanese P, Sato K, Scheltema RA, de Laat W, Knipscheer P, Dekker NH, Groth A, Mattiroli F. CAF-1 deposits newly synthesized histones during DNA replication using distinct mechanisms on the leading and lagging strands. Nucleic Acids Res 2023; 51(8): 3770–92
32. Li T, Fu J, Zeng Z, Cohen D, Li J, Chen Q, Li B, Liu XS. TIMER2.0 for analysis of tumor-infiltrating immune cells. Nucleic Acids Res 2020; 48(W1): W509–W514
33. Li T, Fan J, Wang B, Traugh N, Chen Q, Liu JS, Li B, Liu XS. TIMER: a web server for comprehensive analysis of tumor–infiltrating immune cells. Cancer Res. 2017; 77(21): e108–e10
34. Li B, Severson E, Pignon JC, Zhao H, Li T, Novak J, Jiang P, Shen H, Aster JC, Rodig S, Signoretti S, Liu JS, Liu XS. Comprehensive analyses of tumor immunity: implications for cancer immunotherapy. Genome Biol. 2016; 17(1): 174
35. Győrffy B. Integrated analysis of public datasets for the discovery and validation of survival-associated genes in solid tumors. Innovation (Camb) 2024; 5(3): 100625
36. Győrffy B. Transcriptome-level discovery of survival-associated biomarkers and therapy targets in non-small-cell lung cancer. Br J Pharmacol 2024; 181(3): 362–374
37. Batista IAA, Helguero LA. Biological processes and signal transduction pathways regulated by the protein methyltransferase SETD7 and their significance in cancer. Signal Transduct Target Ther 2018; 3: 19
38. Chiang CY, Fan S, Zheng H, Guo W, Zheng Z, Sun Y, Zhong C, Zeng J, Li S, Zhang M, Xiao T, Zheng D. Methylation of KRAS by SETD7 promotes KRAS degradation in non-small cell lung cancer. Cell Rep 2023; 42(9): 113003
39. Smith S, Stillman B. Purification and characterization of CAF-I, a human cell factor required for chromatin assembly during DNA replication *in vitro*. Cell 1989; 58(1): 15–25
40. Kaufman PD, Kobayashi R, Kessler N, Stillman B. The p150 and p60 subunits of chromatin assembly factor I: a molecular link between newly synthesized histones and DNA replication. Cell 1995; 81(7): 1105–1114
41. Zhang Y, Yang Y, Qiao P, Wang X, Yu R, Sun H, Xing X, Zhang Y, Su J. CHAF1b, chromatin assembly factor-1 subunit b, is essential for mouse preimplantation embryos. Int J Biol Macromol 2022; 195: 547–557
42. Chuikov S, Kurash JK, Wilson JR, Xiao B, Justin N, Ivanov GS, McKinney K, Tempst P, Prives C, Gamblin SJ, Barlev NA, Reinberg D. Regulation of p53 activity through lysine methylation. Nature 2004; 432(7015): 353–60
43. Chiang C, Yang H, Zhu L, Chen C, Chen C, Zuo Y, Zheng D. The epigenetic regulation of nonhistone proteins by SETD7: new targets in cancer. Front Genet 2022; 13: 918509
44. Wang Z, Petricca J, Liu M, Zhang S, Chen S, Li M, Besschetnova A, Patalano S, Venkataramani K, Siegfried KR, Macoska JA, Han D, Gao S, Vedadi M, Arrowsmith CH, He HH, Cai C. SETD7 functions as a transcription repressor in prostate cancer via methylating FOXA1. Proc Natl Acad Sci USA 2023; 120(33): e2220472120
45. Chen Y, Yang S, Hu J, Yu C, He M, Cai Z. Increased expression of SETD7 promotes cell proliferation by regulating cell cycle and indicates poor prognosis in hepatocellular carcinoma. PloS one 2016; 11(5): e0154939
46. Fu J, Huang Y, Xian L. LncRNA SNHG15 regulates hypoxic-ischemic brain injury via miR-153–3p/SETD7 axis. Histol Histopathol 2022; 37(11): 1113–1125